https://doi.org/10.5194/amt-2019-172
Preprint. Discussion started: 12 June 2019

Atmospheric Measurement Techniques
Discussions

Cloud Aerosol Transport System (CATS) 1064 nm Calibration and Validation

Rebecca M. Pauly[1], John E. Yorks[2], Dennis L. Hlavka[1], Matthew J. McGill[2], Vassilis Amiridis[3], Stephen P. Palm[1], Sharon D. Rodier[4], Mark A. Vaughan[5], Patrick A. Selmer[1], Andrew W. Kupchock[1], Holger Baars[6], Anna Gialitaki[3]

[1]Science Systems and Applications Inc., Lanham, 20706, United States
[2]NASA Godard Space Flight Center, Greenbelt, 20771, United States
[3]National Observatory of Athens, Institute for Astronomy, Astrophysics, Space Application and Remote Sensing, Athens, Greece
[4]Science Systems and Applications Inc., Hampton, 23666, United States
[5]NASA Langley Research Center, 23618, United States
[6]Leibniz Institute for Tropospheric Research (TROPOS), Leipzig, Germany

Correspondence to: Rebecca Pauly (rpauly90@gmail.com)

Abstract. The Cloud-Aerosol Transport System (CATS) lidar on board the International Space Station (ISS) operated from 10 February 2015 to 30 October 2017 providing range-resolved vertical backscatter profiles of Earth's atmosphere at 1064 and 532 nm. The CATS instrument design and ISS orbit lead to a higher 1064 nm signal to noise ratio than previous space based lidars, allowing for direct 1064 nm calibration using the molecular normalization technique. Nighttime CATS Version 3-00 data were calibrated by normalizing the signal between 22-26 km above mean sea level to molecular profiles derived from the Modern-Era Retrospective analysis for Research and Applications, Version 2 (MERRA-2) re-analysis data. This altitude region was chosen primarily because the CATS data frame is -2 to 28 km AMSL due to the high CATS laser repetition rate. While this altitude region provides sufficient molecular scattering for the Rayleigh normalization technique, the aerosol loading in this altitude region must be quantified to improve the accuracy of the CATS nighttime calibration. Daytime CATS Version 3-00 data were calibrated through comparisons with nighttime thin, opaque, cirrus cloud layer integrated attenuated total backscatter (iATB).

The CATS nighttime 1064 nm attenuated total backscatter (ATB) uncertainties for clouds and aerosols are primarily related to the uncertainties in the Rayleigh normalization technique, which are estimated to be 7-10%. Median CATS V3-00 1064 nm ATB relative uncertainty at night within cloud and aerosol layers is 7%, consistent with these calibration uncertainty estimates. CATS median daytime 1064 nm ATB relative uncertainty is 21% in cloud and aerosol layers, similar to the estimated 16-18% uncertainty in the CATS daytime cirrus cloud calibration transfer technique. Coincident daytime comparisons between CATS and the Cloud Physics Lidar (CPL) during the CATS-CALIPSO Airborne Validation Experiment (CCAVE) project show good agreement in mean ATB profiles for clear-air regions. Eight nighttime comparisons between CATS and the Polly^{XT} ground based lidars also show good agreement in clear-air regions between 3-12 km, with CATS having a mean ATB of 19.7 % lower than Polly^{XT}. Agreement between the two instruments (~7%) is even better within an aerosol layer. Six-month comparisons of nighttime ATB values between CATS and the Cloud-Aerosol Lidar with Orthogonal Polarization (CALIOP) also show that iATB comparisons of opaque cirrus clouds agree to within 19%. Overall, CATS has demonstrated that direct calibration of the 1064 nm channel is possible from a space based lidar using the molecular normalization technique.

1 Introduction

Lidar plays a crucial role in observing the Earth's atmosphere as it enhances our understanding of the roles clouds and aerosols play in the climate system by providing vertical profiles of backscatter coefficient and other optical properties. Lidar have been utilized to study aerosols (e.g. McGill et al., 2003, Papayannis et al., 2009, Haarig et al., 2017, Rajapakshe et al., 2017, Lee et al., 2018) and clouds (e.g. Yorks et al., 2011, Avery at al., 2012, Haarig et al., 2016, Noel et al., 2018) in numerous studies to derive layer and optical property information. Lidar, particularly from a spaceborne platform, has the capability to provide these vertical profiles of cloud and aerosol optical properties globally.

To derive optical properties of clouds and aerosols from backscatter lidar systems, the signal must be accurately calibrated. Scientists have used various methods for calibrating lidar measured signal, but most are based on the molecular normalization technique described in Russell et al. (1979). Ground based lidars (e.g. Micro-Pulse Lidar Network (MPLNet) (Welton et al., 2001)) calibrate by normalizing their signal to the molecular profile, but require knowledge of the aerosol optical depth of the atmosphere between the instrument and the calibration region (Welton et al., 2002). Sometimes, as is the case for the MPLNet, lidar sites are co-located with Aerosol Robotic Network (AERONET) (Holben et al., 1998) sites. In these cases, the aerosol optical depth can be derived directly from the AERONET column optical depths measured by sun photometers.

High altitude airborne and spaceborne lidars have the benefit of weak aerosol loading in the atmosphere between the instrument and the calibration region. Spaceborne lidars (e.g. Lidar In-Space Technology Experiment (LITE) (Winker et al., 1996), the Geoscience Laser Altimeter System (GLAS) (Spinhirne et al., 2005), and the Cloud-Aerosol Lidar with Orthogonal Polarization (CALIOP) (Winker et al., 2010) have used a similar molecular normalization technique to calibrate their 532 nm signals. Due to differences in the molecular signal to noise ratio (SNR) between 1064 nm and 532 nm for these instruments, calibration techniques for the 1064 nm attenuated total backscatter (ATB) calibration are based on the 532 nm ATB calibration.

Operationally, LITE did not calibrate its 1064 nm channel. GLAS and CALIOP use variants of the cirrus cloud calibration scheme proposed by Reagan et al. (2002). The CALIOP algorithms first calibrate the 532 nm data by normalizing the data between 36-39 km (Kar et al., 2018) to a modeled molecular density profile derived from the Modern-Era Retrospective analysis for Research and Applications, Version 2 (MERRA-2) re-analysis meteorological profiles (Gelaro et al., 2017). The 1064 nm signal is calibrated utilizing the 532 nm calibrated signal within cirrus clouds comprised of relatively large ice crystals. Clouds are identified for use in the calibration algorithm based on thresholds applied to the magnitude of the 532 nm layer-integrated attenuated backscatter, cloud base and top altitudes, cloud temperature, and the layer-integrated 532 nm volume depolarization ratio (Vaughan et al., 2019). Using cirrus comprised of large ice crystals ensures that the in-cloud backscatter coefficients at 1064 nm and 532 nm are essentially identical (Reagan et al., 2002, Vaughan et al., 2010, Haarig et al., 2016), thus enabling calculation of a 532-to-1064 calibration scale factor for each qualifying cirrus cloud identified in the CALIPSO backscatter data. These calibration scale factors are then composited into a continuous time history using a two-dimensional moving window averaging scheme that spans multiple orbits. For any individual profile, the CALIPSO 1064 nm calibration coefficient is simply the product of the interpolated instantaneous value of the scale factor time history and the corresponding 532 nm calibration coefficient (Vaughan et al., 2019).

The Cloud-Aerosol Transport System (CATS) (McGill et al. 2015) onboard the International Space Station (ISS) is unique in that its strong nighttime SNR at 1064 nm enables calibration of the 1064 nm nighttime data directly by normalizing the range corrected signal to a modeled molecular profile. There are three factors that enable the direct calibration of CATS 1064 nm data. First, CATS utilizes photon counting detectors that provide sufficient detection sensitivity at 1064nm (Yorks et al., 2016a). Second, the combination of low pulse energies (1-2 mJ) and higher repetition rate (4-5 kHz) lead to a higher output power (~8W) than all previous spaceborne lidars. Third, the CATS orbit on the ISS is considerably lower than other spaceborne lidars at ~405 km above mean sea level (AMSL). Section 2 of this paper discusses the CATS instrument, algorithms, and calibration. Section 3 discusses the uncertainties in the CATS calibration coefficients and attenuated total backscatter (ATB) measurements.

Comparisons with airborne, ground-based, and space-borne lidar are presented in Sect. 4. Concluding remarks are given in Sect. 5.

2 The CATS Instrument

CATS is an elastic backscatter lidar onboard the ISS, which operated nearly continuously from 10 February 2015 to 30 October 2017. With the ISS 51° inclination orbit, CATS provided diurnally varying measurements of clouds and aerosols. Over the course of the CATS lifetime, it operated in two modes. The first, mode 7.1, featured two fields-of-view with backscatter and depolarization information at both 1064 nm and 532 nm. CATS operated in mode 7.1 for only 40 days due to a failure in laser 1 electronics, after which operations switched to mode 7.2. Mode 7.2 featured a single field of view, backscatter profiles at 1064 and 532 nm, and depolarization measurements at 1064 nm. Since the majority of the CATS data was collected in mode 7.2, this paper primarily focuses on results from mode 7.2, although the calibration process is the same for both.

CATS Version 3-00 data products, which are the focus of this paper, consist of two primary data processing levels. To create Level 1 (L1) data products, the raw CATS signal is range corrected, geolocated, corrected for detector non-linearity, and normalized to laser energy, producing the normalized relative backscatter (NRB). The NRB can be defined as:

$$NRB(r) = \frac{\{[N_S(r)*D]-N_B\}r^2}{E}, \qquad (1)$$

where r is the range, N_s is the geolocated CATS signal, D is the correction term for detector non-linearity, and E is the laser energy. Since the detectors employed by CATS have a deadtime of 28 to 30 ns for a discriminator maximum count rate on the order of 30 MHz, and CATS has a photon count rate of less than 35 MHz 99% of the time below 28 km, D is less than 1.10 for most atmospheric profiles (Yorks et al., 2016b). N_B is the photon counts from solar background which can be determined by averaging the signal acquired after the signal attenuated by Earth's surface. Next, the signal is calibrated using the molecular profile derived from MERRA-2 meteorological re-analysis data. For Level 2 (L2) data products, aerosol and cloud layers are detected and optical properties are determined. Descriptions of the L2 algorithms are beyond the scope of this paper, but more information about both L1 and L2 processing algorithms can be found in the CATS Algorithm Theoretical Basis Document (ATBD) (Yorks et al., 2016b).

2.1 CATS Nighttime Calibration

CATS exhibits high nighttime 1064 nm SNR, enabling 1064 nm attenuated total backscatter (ATB) direct calibration without any dependence on the CATS 532 nm signal. Fig. 1 shows the CATS 1064 nm SNR for both night and day as compared to those of CALIOP 1064 nm. The CATS nighttime SNR is on average approximately an order of magnitude higher than that of CALIOP throughout the measurement column. On the other hand, the daytime CATS SNR is approximately a factor of 2 lower than CALIOP's, necessitating a different calibration technique for daytime data, as described in Section 2.2. The CATS nighttime signal is calibrated in the region between 22-26 km AMSL. There are two factors that determined this altitude region: (1) the CATS data frame is -2 to 28 km AMSL because the CATS laser 1 repetition rate of 5 kHz creates a 30 km atmospheric window for scattering from a single laser shot, and (2) testing of the highest possible altitude regions (based on #1) showed better performance in the 22-26 km than the 23-27 km region. While this altitude region provides sufficient molecular scattering for the Rayleigh normalization technique, the aerosol loading in the lower stratosphere (22-26 km) is also higher than the 36-39 km region used to calibrate 532 nm CALIOP data. To improve the accuracy of the CATS nighttime calibration, the aerosol loading in the calibration region must be quantified, along with the ozone transmission profile, molecular backscatter profile, and polarization gain ratio (PGR). Additionally, the background signal must be removed from the data.

The nighttime Rayleigh normalization technique is complicated by molecular folding of the raw signal caused by CATS' high repetition rate laser. Molecular folding refers to the fact that the CATS raw photon count at altitude, z, where z< 28 km, has scattering contributions from the atmosphere at heights z+Nx. N=1,2,3, etc., where x equals 37.5 km for mode 7.2 since laser 2 had a repetition rate of 4 kHz. The implications of this are that the region below the surface return (from -2.5 to -4.5 km), which is used for determining the background signal, also has molecular signal from 33 to 35 km. If this folded signal is not removed from the background signal, most of the signal in the calibration region will be removed by the background removal process. A correction term was implemented to account for this molecular folding. The folded signal is computed from instrument parameters and the known molecular attenuated backscatter cross section between 33 km and 35 km and subtracted from the signal in the background region (2.5 to 4.5 km below the ground). For nighttime data, this can affect the profile slope of the average signal above 20 km. If too much folding is removed, the slope will be greater than the molecular slope and if too little is removed, the average signal slope will be less than the molecular slope. In the data processing, a scaling factor in the folding equation is adjusted until the slope difference is less than 3.5%. The potential error introduced by this correction is discussed further in Sect. 3. For more information about molecular folding corrections, see the CATS ATBD (Yorks et al., 2016b).

Depending on the profile location of the calibration region, the aerosol loading at those altitudes can introduce uncertainties in the computation of the calibration coefficient of any lidar system (Powell et al., 2009, Vernier et al., 2009, Kar et al., 2018). Thus, the CATS calibration algorithm incorporates an aerosol scattering ratio (R) to improve the accuracy of the calibrated signal. No space-based sensors provide aerosol scattering ratios at 1064 nm on a global scale. However, since CALIOP V4 Level 1 data provides a robust estimate of the 532 nm scattering ratios in the CATS vertical calibration zone, the CALIOP data is used to estimate the spatially and temporally varying 1064 nm scattering ratio at these altitudes (Fig. 2). Every 15 days, the CATS team computes 30-day averages of the CALIOP 532 nm scattering ratios between 22 and 28 km. The 1064 nm scattering ratio is then computed from the 532 nm scattering ratios, which have been interpolated to the CATS vertical resolution, using

$$R_{1064}(r) = 1 + \frac{\chi_P \beta_{M,532}(r)(R_{532}(r)-1)}{\beta_{M,1064}(r)}, \tag{2}$$

where β_M at 532 and 1064 nm are the computed Rayleigh backscatter coefficients and χ_P is the backscatter color ratio defined by Hair *et al.* (2008) as,

$$\chi_P = \frac{\beta_{P,1064}(r)}{\beta_{P,532}(r)} = 0.4. \tag{3}$$

The ozone transmission, $T^2{}_o(r)$, is determined from the MERRA-2 ozone mass mixing ratios and meteorological profiles. The ozone transmission is calculated using

$$T_o^2(\lambda, r) = exp\left[-2c_o(\lambda) \int_H^r \varepsilon_o(r')dr'\right], \tag{4}$$

where $\varepsilon_O(r)$ is the column density of ozone and $c_O(\lambda)$ is the Chappius ozone absorption coefficient in cm^{-1} obtained from a lookup table found in Iqbal (1984). The 1064 nm ozone coefficient is ~0.0 cm^{-1} leading to the ozone transmission at 1064 nm being 1.0 and negligible to the 1064 nm signal calibration.

The molecular backscatter coefficient is calculated using the relationship to atmospheric temperature and pressure (Collins and Russell,1976), with

$$\beta_M = \frac{p}{KT}(5.45x10^{-32})\left(\frac{\lambda}{550}\right)^{-4.09} \quad , \tag{5}$$

where T is temperature, p is the atmospheric pressure, and K is the Boltzmann constant. The atmospheric profiles of temperature and pressure are obtained from the MERRA-2 re-analysis data. The atmospheric profiles are interpolated to the 60 m vertical resolution of the CATS lidar backscatter data. The molecular extinction coefficient (σ_M) is determined though the relationship:

$$\sigma_M = \beta_M\left(\frac{8}{3}\right)\pi \tag{6}$$

The PGR is required to account for relative gain between the CATS parallel and perpendicular channels in the receiver. The PGR is determined from the reflected solar background radiation ratio of the parallel-to-perpendicular channels from dense cirrus clouds following the methodology from Liu et al. (2004). It can be assumed that the difference in solar background counts between the two channels is negligible because scattered solar radiation from dense ice clouds is unpolarized (Liou et al., 2000). The PGR is computed through the ratio of the sum of all parallel and perpendicular profiles in a daytime granule containing dense ice clouds meeting the following criteria:

1) Mid-cloud temperature < -35 C
2) Cloud layer integrated ATB (iATB): $0.008 < \text{iATB} < 0.044$ sr^{-1}
3) Layer integrated depolarization ratio (δ_{1064}): $0.3 < \delta_{1064} < 0.8$

   where:

$$\delta_{1064} = \frac{\sum_{layer} NRB_{perp}}{\sum_{layer} NRB_{par}} \tag{7}$$

4) Cloud optical depth > 1.75

These criteria were only used to identify cirrus clouds that would be suitable for calculating the PGR. Historical calibration coefficients and PGR values were used to estimate iATB, depolarization ratio, and optical depth. These historical values were not applied to the raw data during the actual PGR calculation. Because the CATS instrument ceased operation prior to the processing of CATS V3-00 data, a singular yearly average PGR value was used for 2015, 2016, and 2017 equaling 0.9839, 0.9768, and 0.9708 respectively. The PGR is applied as a multiplicative factor to the perpendicular channel NRB data. The perpendicular and parallel NRB data are added together to arrive at the total NRB.

To prepare for calibration, the CATS night files, or granules, are separated into six segments averaging 7.8 minutes each, depending on the length of the granule. Granules are the files for the CATS data that span about half of the ISS orbit and contain only daytime or only nighttime observations. For calibration, the total NRB profile is averaged within each segment.

The average total NRB profile is divided by the ozone transmission and scattering ratio of the corresponding wavelength as a function of height. The profiles of calibration coefficient (C) for each segment within a file are determined by normalizing the mean NRB signal which has been corrected for aerosol loading and the ozone transmission, β_{CN}, to the mean molecular backscatter ($\beta_M T^2_M$) (Russell *et al.* 1979, Del Guasta 1998, McGill *et al.* 2007, Powell *et al.* 2009), via

$$\mathrm{C}_\lambda(\mathrm{r}) = \frac{\left[\frac{\mathrm{NRB(r)}}{\mathrm{T_O^2(r)}R(\mathrm{r})}\right]}{\beta_\mathrm{M}(\mathrm{r})\mathrm{T_M^2(r)}} = \frac{\beta_\mathrm{CN}(\mathrm{r})}{\beta_\mathrm{M}(\mathrm{r})\mathrm{T_M^2(r)}}, \tag{8}$$

The final calibration coefficient for the segment is the average coefficient in the calibration region profile (i.e. an average of C(r) from 22 to 26 km). Each coefficient is compared to minimum and maximum thresholds to determine if the calculated value is within acceptable bounds. If the coefficient is not, it is discarded, and not used in the final calibration calculation. The calibration thresholds were determined through prior experience calibrating airborne lidar as well as through testing on CATS data during which outliers that negatively impacted the overall calibration were identified. All good calibration values within a file are then averaged. On average, 60-70% of calibration values within a given granule are accepted and used for determining the final calibration coefficient for that file. If less than 15% of calibration values are accepted, a default calibration coefficient is used for that granule, computed as the mean of the calibration coefficients from the previous week of data. These files represent 3% of CATS data, typically when the laser was recently turned on after being off for more than 2 hours, and are consistent with the nighttime files flagged as having poor depolarization quality in the CATS data products. The final calibration coefficient is then applied to all NRB profiles within the granule to compute the ATB.

The CATS nighttime calibration coefficients were found to have an oscillating change in values over time ranging on average from $4\text{x}10^8$ to $1.4\text{x}10^9$. The oscillating change in calibration values are attributed to the changing of the sun's angle with respect to the ISS orbital plane, known as its beta angle. The amount of sunlight and solar heating CATS received was monitored by the cold plate temperature. The cold plate is a component of the optical system that during Mode 7.2 operation was not receiving any heat from the instrument itself, making it a good indicator of the amount of heat received from the sun. Fig. 3 shows the daily average calibration coefficient and CATS cold plate temperature from January- April 2016. The changing value of the calculated calibration coefficient follows the same pattern as the cold plate temperature. The two values have a correlation coefficient of 0.8066.

2.2 CATS Daytime Calibration

Because CATS daytime data exhibits lower SNR due to noise introduced by the solar background, calibrating the daytime granules through the normalization method is not possible. Therefore, the daytime calibration coefficients are determined through calibration transfer from the nighttime calibration (Eq. 9). In previous CATS data versions, the daytime calibration was determined through a manual normalization to the Rayleigh signal that required periodic assessment and updates. In the latest CATS release, version 3-00, a singular daytime calibration coefficient was determined for each month of CATS data through an assessment of the iATB in strongly scattering opaque cirrus clouds that have a mid-layer temperature colder than -20° C and a layer integrated depolarization ratio between 0.25 and 0.7. Physically thin clouds were used to ensure that only strongly scattering clouds were used in the assessment.

It was found that using a month of data provided enough data points to compute a calibration value while also reasonably capturing the temporal variability of calibration coefficients. The assessment of cirrus cloud properties was done using V2-01 CATS data in which the layer detection and optical properties algorithms were already run. A layer is classified as opaque if no layer or ground signal is detected below it. The iATB is calculated through the cloud until the point of signal attenuation. In physically thin, opaque cirrus clouds, there should be little difference between nighttime and daytime iATB retrievals. This characteristic of cirrus clouds has been observed in CALIOP data as shown in Young et al. (2018). Young et al.'s CALIOP comparisons of opaque cirrus at 532 nm showed substantial iATB similarities for both nighttime and daytime measurements, with a peak iATB of ~0.03 sr^{-1} in both cases. Given that there is relatively little difference in the backscatter from cirrus clouds between 532 nm and 1064 nm (Vaughan et al., 2010, Haarig et al., 2016), one would expect that the daytime and nighttime iATB distributions from 1064 nm retrievals should also be similar.

The daytime calibration coefficient is shown as

$$C_{day} = \left. \frac{1}{N_{day}} \sum_{k=1}^{N_{day}} iNRB_k \middle/ \frac{1}{N_{night}} \sum_{k=1}^{N_{night}} iATB_k \right. , \tag{9}$$

where both the nighttime iATB and daytime iNRB were computed over each month of CATS data. The left panel of Fig. 4 demonstrates the CATS daytime calibration for the month of August 2016. In the CATS V2-01 data, the daytime cirrus iATB distribution is shifted higher than the nighttime distribution, with a peak at 0.05 sr^{-1}. For the V3-00 CATS processing, the daytime calibration coefficient for August 2016 was increased from $6x10^8$ to $9x10^8$ and was applied to all August 2016 daytime granules. As seen in the right panel of Fig. 4, this change resulted in the peak of the daytime cirrus iATB distribution moving to ~0.03 $km^{-1}sr^{-1}$ with better agreement with the nighttime distribution. Overall, it was found that a change of ~$1x10^8$ in the calibration coefficient results in a shift of ~0.01 sr^{-1} in the iATB. This method was applied to all CATS mode 7.2 daytime data in V3-00. Changes in the nighttime cirrus iATB distributions between versions are attributed to improvements in the layer type classifications within the L2 processing (Yorks et al., in prep.).

Overall, this daytime calibration method results in average biases of the mean, median, and mode daytime iATB value with respect to nighttime of 0.000168, -001215, and -0.00258, respectively (Table 1), which are each less than a 10% bias. The mean absolute error (MAE) values also indicate that, overall, the distribution statistics between night and day granules are similar, with MAE values equating to 8-13% error in the peak of the distribution and 17% error in the standard deviation of the distribution. Since the daytime calibration coefficient is directly related to the nighttime calibration coefficient, it yields similar a change in values over time as the nighttime calibration coefficient (Fig. 3), but as a step function given it is computed every month and not every granule.

3 Error Analysis

There are two types of error that contribute to the uncertainty in the CATS calibration: systematic and random errors. There are four sources of uncertainty included in the systematic error calculation (Yorks et al., 2016b). They are: uncertainties in the scattering ratios (R) at 22-26 km from CALIOP, including assumptions of backscatter color ratio, uncertainties in the molecular backscatter (β_M) computed from MERRA-2 data, uncertainty in the modeled two-way transmittance (T^2) from atmospheric molecules and ozone, and errors introduced by the CATS optical system. The optical system error can be reduced through corrections such as deadtime correction and energy normalization to less than 0.1% and is therefore negligible. The total systematic error in the calibration, following the method outlined by Powell et al. (2009), can be defined as

$$\left(\frac{\Delta C}{C}\right)_{sys}^2 = \left(\frac{\Delta R}{R}\right)^2 + \left(\frac{\Delta\beta_M}{\beta_M}\right)^2 + \left(\frac{\Delta T^2}{T^2}\right)^2 , \tag{10}$$

and has been estimated to be 6%. The errors in the molecular backscatter and background transmission are constant, equaling 3% and 0.2% respectively. Regan et al. (2002) estimates uncertainty for the 532 nm molecular backscatter coefficient of 3% and uncertainty at 1064 nm at a nominal cirrus cloud top altitude of 0.2%. Thus, the constant 3% molecular backscatter uncertainty is conservative, and results from uncertainties in GMAO-derived temperatures from the upper troposphere that are estimated to be less than 1 °C (Campbell et al., 2015). Omitting the King factor, which accounts for the anisotropy of molecules, in our molecular backscatter computation could lead to an additional error of 1-3% in the molecular backscatter error (Hostetler et al., 2005). This additional error would lead to less than 1% error in the overall calibration, making is far less important than other factors covered in this paper, especially given that the 1064 nm molecular backscatter uncertainty is likely overestimated. The error in the scattering ratio is computed for each CALIOP scattering ratio file received. The dominant systematic uncertainty in the scattering ratio comes from the uncertainty in the CALIOP nighttime calibration which is estimated to be 1.6% ± 2.4 (Kar et al., 2018). Variability in the scattering ratio from CALIOP is also included in the error estimate of the scattering ratio.

The random error in the CATS calibration is primarily caused by noise in the lidar signal during the calibration normalization. The random error can be determined through the variability of the NRB signal within each calibration segment (Welton and Campbell, 2002) and is calculated through

$$\left(\frac{\Delta C}{C}\right)^2_{ran} = \left(\frac{\left(\frac{stdev(NRB(r))}{\sqrt{N}}\right)}{NRB(r)}\right)^2, \tag{11}$$

where N is the total number of NRB values used. For CATS, the 7.8 min averaging interval equals 9,360 profiles. This averaging interval was chosen because it reduced the random error of each individual calibration value within a granule, but still provided sufficient values (at least 6) to compute the granule mean calibration coefficient. Uncertainties in background subtraction and other CATS correction terms (discussed in Sect. 2) are included in the NRB variability. Typical results for random error in the calibration range from 5-7%. The total error is determined through

$$\left(\frac{\Delta C}{C}\right)^2_{tot} = \left(\frac{\Delta C}{C}\right)^2_{sys} + \left(\frac{\Delta C}{C}\right)^2_{ran} \tag{12}$$

and thus, comes to a total uncertainty in the CATS nighttime calibration (ΔC) of 7-10%.

The daytime calibration uncertainty can be estimated from the variability of the NRB signal and the nighttime calibration error. The nighttime calibration uncertainty already contains the systematic error sources which would also impact the daytime calibration. Since strongly scattering cirrus clouds are used in the daytime calibration, uncertainties in the multiple scattering factor, η, also play a role. Multiple scattering occurs when the incident light from the lidar is scattered by more than one particle in the scattering feature, in this case, the cirrus cloud. Multiple scattering can lead to higher detected signals and is corrected using the appropriate value of η (Platt, 1979, Garnier et al., 2015). For CATS, η for cirrus clouds was determined to be 0.52 through comparisons with the Cloud Physics Lidar (CPL). Since a constant daytime calibration coefficient is determined for each month of CATS data and is based on comparisons with nighttime data, the overall systematic error for the daytime calibration can be estimated to be the same as the average nighttime calibration uncertainty over the month.

The daytime random error is estimated from the variability in the NRB signal. Therefore, the total daytime error can be shown through the equation

$$var(C_{day}) = \left(\frac{1}{N_{day}}\right)^2 \sum_{k=1}^{N_{day}} var(iNRB_{day,k}) + \left(\frac{1}{N_{night}}\right)^2 \sum_{k=1}^{N_{night}} var(iNRB_{night,k}) + \frac{1}{N_{night}} \sum_{k=1}^{N_{night}} (\Delta C_{night,k})^2 \quad . \tag{13}$$

The daytime random error due to the noise in the NRB is estimated to be ~15%, leading to an overall daytime calibration uncertainty of ~16-18%.

The ATB uncertainties are computed using a propagation of errors from the NRB uncertainties. ATB is calculated through

$$ATB = \frac{NRB}{C}. \tag{14}$$

NRB uncertainties ($\varDelta NRB$) are calculated using the methodology outlined in Welton and Campbell (2002). By utilizing a standard propagation of errors from the NRB uncertainty and the calibration uncertainty, the ATB uncertainty was computed and can be expressed as

$$\varDelta ATB = \sqrt{\left(\frac{1}{C}\right)^2 \varDelta NRB^2 + \varDelta C^2 \left(\frac{NRB}{C^2}\right)^2}. \tag{15}$$

As part of the NRB error, there is error associated with the molecular folding correction factor (see Sect. 2.1) which impacts the ATB profile. Since the correction factor acts by matching the slope of the measured signal to that of the modeled molecular profile within the calibration region, the error was assessed through the amount of error introduced lower in the CATS profile for given errors in the calibration region slope. In V3-00, the majority of corrected slopes in the calibration region have an error of less than 3.5%. However, in very few cases, the slope is different from the molecular slope by 10% in the calibration region. The assessment of this "worst case" calibration region slope error showed that the maximum error introduced in the profile is ~4% in the 17-18 km region. The error in the profile then decreases as the signal approaches the surface, introducing ~2% error.

The CATS 1064 nm ATB uncertainties for clouds and aerosols at night are primarily a related to the uncertainties in the Rayleigh normalization technique. Features such as cloud and aerosol layers with higher backscatter intensities tend to have lower ATB uncertainty, while clear air regions, with lower scattering intensity and lower SNR, have higher ATB uncertainty. The median CATS 1064 nm ATB relative uncertainties from the Mode 7.2 V3-00 data products within cloud and aerosol layers are 7% at night and 21% during daytime. For clear-air regions, there is large variability (20% to over 100%) in the CATS 1064 nm ATB relative uncertainties, since the SNR varies as a function of altitude at night due to molecular scattering and scene during daytime due to the noise introduced from the solar background.

4 Data Comparisons

4.1 Airborne Lidar Comparisons

During the CATS-CALIOP Airborne Validation Experiment (CCAVE) in August 2015, the NASA ER-2 conducted several ISS under flights. As part of the CCAVE payload, CPL was able to collect coincident data with CATS. CPL is an airborne backscatter lidar that has participated in over thirty field campaigns, including several satellite instrument validation projects (McGill et al., 2002). CPL data products include ATB from both 1064 and 532 nm. Similar to nighttime CATS data, CPL is calibrated by normalizing the signals acquired between 15 km and 17 km to a modeled molecular attenuated backscatter profile derived from MERRA-2 reanalysis data. A scattering ratio of 1.27 is applied in the calibration region, based on the work of Vaughan et al. (2010), and the estimated aerosol loading within a standard atmospheric profile in the northern hemisphere.

Fig. 5 shows the coincident flight from the CCAVE project which occurred at 01:37 UTC on 7-8 August 2015 during the day over western Nevada. CPL flew beneath CATS with clear sky conditions, although this scene is made more complicated due to variations in the terrain and background smoke aerosols due to wildfires in the region, as can be seen in the curtain plot (Fig. 5-left). The CATS average is comprised of 165 profiles which spans 55 km, and is calibrated using the daytime cirrus cloud calibration transfer technique. The CPL mean profile is an average of 280 profiles. Despite the complicated terrain and smoke, the mean ATB profiles from CATS and CPL still shows good agreement in the clear sky region above the smoke, with the average CPL and CATS mean ATB between 7-15 km equal to 4.1927x10^{-5} [km^{-1}sr^{-1}] and 4.0972x10^{-5} [km^{-1}sr^{-1}] respectively, meaning the CATS average ATB was 2.28% below CPL. This agreement is surprising since the CATS daytime calibration uncertainty is ~16-18%, but this case occurred near local twilight when CATS SNR is higher.

Another daytime underpass occurred at 20:31 UTC on 20 August 2015 over northern Utah near Great Salt Lake. The CPL curtain plot and the mean ATB profile from both CATS and CPL centered around the overpass time can be seen in Fig. 6. The CPL data was averaged to six minutes (360 ATB profiles) which covers a distance of about 70 km. The CATS data were averaged over the same distance and is comprised of 210 ATB profiles, and like the 7-8 August 2015 case is calibrated using the daytime cirrus cloud calibration transfer technique. As shown in the CPL curtain plot, the underpass segment was in clear-sky conditions (no clouds) with a well-defined smoke aerosol layer from nearby wildfires. Both instruments observed the top of this aerosol layer around 5 km AMSL. The differences in SNR are also apparent as the CATS profile is noisier than the CPL profile. The average CPL ATB value between 7-15 km was 4.2967x10^{-5} [km^{-1}sr^{-1}] and the average CATS ATB was 5.1939x10^{-5} [km^{-1}sr^{-1}], 20.88% higher than CPL. These differences are expected given the 16-18% CATS daytime calibration uncertainty.

The greater noise in the CATS signal on the 20 August case should be noted as compared to the 7-8 August case. This is likely attributed to the different times of day the two flights occurred. The 7-8 August flight occurred in the early evening, which will minimize the noise induced by solar background due to the lower sun angles, while the 20 August flight occurred closer to local noon, which will maximize noise from sunlight. Some of the differences in the ATB signal within the PBL aerosol layers can be attributed to spatial inhomogeneity within the aerosol plumes and the temporal difference in the measured profiles. For both under-flights, the error in the CATS ATB compared with CPL is well within the CATS daytime uncertainty estimates discussed in Sect. 3.

4.2 Ground-based Comparisons

In addition to the coincident airborne CPL data, CATS was also compared to ground-based systems. CATS frequently passed over (or close to) the European Aerosol Research Lidar Network (EARLINET) sites. The Polly^{XT} lidar (Baars et al., 2016; Engelmann et al., 2016) is a Raman lidar developed by at the Leibniz Institute for Tropospheric Research (TROPOS), Leipzig, Germany and is used at some EARLINET sites. The Polly^{XT} systems emit laser pulses at 1064, 532, and 355 nm with elastic backscatter detectors at each wavelength, as well as Raman channel detectors at 386.73 and 607.4 nm. There are Polly^{XT} lidars all across Europe as part of the EARLINET, but only data collected from the Leipzig, Germany (51.3N; 12.4E) and the Athens NOA (National Observatory of Athens) (37.97 N; 23.71 E) sites were used in this study.

Raw EARLINET data are processed through the Single Calculus Chain (SCC) (D'Amico et al., 2015). The first part of the SCC is the EARLINET Lidar Pre-Processor (ELPP) where the raw lidar signal is range and deadtime corrected, the background signal is subtracted, and molecular extinction and transmission profiles are computed from meteorological radiosonde data or the standard atmosphere (D'Amico et al., 2016). The second part of the SCC is the EARLINET Lidar Data Analyzer (ELDA) (Mattis et al., 2016). In the ELDA the backscatter coefficients, extinction coefficients, and lidar ratio are derived. During the backscatter coefficient calculation, the EARLINET data is calibrated by normalizing it to the molecular using an assumed aerosol free region, which is determined by the ELDA algorithms.

Using the particulate backscatter and particulate extinction profiles derived from the Polly^{XT} data, "CATS-like" ATB profiles were calculated following the methodology outlined in Mona et al. (2009) where the attenuated backscatter coefficient can be defined as

$$\beta'(z) = \beta_{tot}(z)T_{par}^2(z)T_M^2(z). \quad (16)$$

β_{tot} is the total backscatter coefficient comprised of contributions from particles, molecules, and ozone. T_{par}^2 is the particulate transmittance and is calculated through

$$T_{par}^2(z) = exp\left(-2\int_z^{z_s}\alpha_{par}(\zeta)d\zeta\right), \quad (17)$$

where α_{par} is the particulate extinction and z_s is the CATS altitude. The particulate backscatter was computed from the 1064 nm and 607 nm signals through the methodology described in Proestakis et al. (2019). The uncertainty in the backscatter coefficient retrieval is estimated to be between 5-20% (Ansmann et al., 1992; Whiteman et al., 2003; Povey et al., 2014). The particulate extinction coefficient was calculated using the Klett method (Klett, 1981; Fernald, 1984) using assumed lidar ratios between 30 - 35 sr. Sun photometer data was used, wherever possible, to estimate the lidar ratio. The molecular signal and attenuation profiles were computed from the temperature and pressure profiles found within the CATS L1B HDF5 file corresponding to the overpass.

Fig. 7 shows the mean ATB profiles from the nighttime CATS overpass of the Leipzig Polly^{XT} site on 24 September 2015 at 01:13:34 UTC. CATS passed 31 km from the Leipzig site. The mean profiles consist of fourty CATS ATB profiles (~10 km) and thirty minutes of Polly^{XT} data. This difference in number of averaged profiles is a contributing factor to the difference in the noise between the two instrument profiles. The CATS mean ATB profile was 7.7 % higher than the Polly^{XT} mean signal

https://doi.org/10.5194/amt-2019-172
Preprint. Discussion started: 12 June 2019

between 3-12 km. Another nighttime overpass, shown in Fig. 8, occurred on 30 July 2015 at 00:18:19 UTC ~41 km away from the Leipzig site. In this overpass, CATS ATB was 14.1% lower than the Polly^{XT} data between 3-12 km.

Overall, eight clear-sky, nighttime overpasses were used in this analysis. The average difference from 3-12 km between CATS and Polly^{XT} ATB was 19.7% with an average CATS distance from the Polly^{XT} site of 40 km (Fig. 9). Fig. 9 also shows the CATS and Polly^{XT} ATB scatter plot from all eight overpasses. The correlation coefficient between the two instrument retrievals is 0.75. The difference between the two instruments falls within the uncertainties in the CATS ATB (Sect. 3) and the uncertainties in the Polly^{XT} retrievals. In addition to the clear sky comparisons, one overpass which had strong aerosol scattering within the planetary boundary layer (PBL) was assessed. The center-most 1.25 km of the PBL depth retrievals were compared to avoid spatial inhomogeneities in the PBL top and ground height. CATS underestimated Polly^{XT} by 7%, supporting the ATB uncertainty assessment in Sect. 3 of lower ATB uncertainties (~8%) within stronger backscattering layers. Given the high SNR of CATS 1064 nm nighttime signal (Fig. 1), these differences can be primarily attributed to the 7-10% uncertainty in the CATS nighttime Rayleigh normalization calibration technique.

Previous studies have investigated the validity of using EARLINET for spaceborne lidar validation (Mamouri et al., 2009; Papagiannopoulos et al., 2016; Proestakis et al., 2019) and have found it is a useful method for lidar validation. A major source of the variability between the ground-based and spaceborne measurement results was found to be the variances in the atmospheric scene observed due to the spatial and temporal differences in the measurements. In a CALIOP validation study by Mamouri et al. (2009), it was found that for comparisons where the over pass was within 100 km from the EARLINET site the variability of the aerosol loading introduced a discrepancy on the order of 5%.

4.3 CALIOP Comparison

In addition to coincident data, statistical comparisons with CALIOP measurements can be used to further assess the CATS calibration. However, differences in instrument design can make the interpretation of these comparisons somewhat challenging. CALIOP measures the total backscatter in the 1064 nm channel using a single avalanche photodiode (APD), which simultaneously delivers a desirable high quantum efficiency and a less desirable high dark noise count rate that has been increasing linearly over the course of the mission (Hunt et al., 2009). CATS, on the other hand, uses a pair of photon counting modules to separately measure the 1064 nm backscatter components polarized parallel and perpendicular to the polarization plane of the CATS laser. The difference in detector performance is illustrated in Fig. 10, which shows the occurrence frequencies of the attenuated backscatter coefficients measured by CATS and CALIOP between 1 April and 30 September 2016 at all latitudes between 51.8° N and 51.8° S. This comparison was designed to investigate distributions of cirrus cloud backscatter intensity, so the data are restricted to nighttime measurements extending from 0 to 5 km above the point where the atmospheric temperature in any profile first drops below –40° C.

Because CATS uses photon counting detectors, the molecular backscatter signals in the CATS distribution appear as a sharp, well-confined peak at ~2.5×10^{-5} km^{-1} sr^{-1}. The substantial broadening of the CALIOP distribution in this region is a consequence of the high APD dark noise levels in the CALIOP detectors. The distributions begin to converge above ~0.008 km^{-1} sr^{-1}, although the CATS occurrence frequencies remain persistently lower than CALIOP throughout. Approximately 99.7% of all attenuated backscatter coefficients measured for both lidars lie below 0.025 km^{-1} sr^{-1}. Some of the differences at higher ATB values may be a consequence of the fact that these are not coincident measurements; because the two instruments fly in very different orbits, they sample different regions of the atmosphere at different times of day. CALIPSO flies in a sun-synchronous 98° orbit with a 16-day repeat time, and thus CALIOP measurements are acquired at essentially the same time of day at any given location along the orbit track (Hunt et al., 2009). The ISS flies in a 52° precessing orbit with a 3-day repeat time, so that CATS measurements at identical locations will occur at many different times of the day. This precessing orbit allows CATS data to be used to assess the diurnal variability of clouds and aerosols.

To avoid the confounding effects introduced by APD dark noise contamination of the weaker signals measured by CALIOP, a second study was conducted comparing the iATB from opaque cirrus detected by the two sensors. This study used CATS and CALIOP data acquired between 1 March and 31 December 2016, with the latitude range once again confined to between 51.8° N and 51.8° S. The following cloud selection criteria were applied uniformly to both data sets.

(a) All layers must be classified as opaque ice clouds and be the uppermost (and only) layer in the column.
(b) All layers must be detected at a nominal 5-km horizontal averaging resolution.
(c) The mid-layer temperature for all layers must lie below –37° C (see Campbell et al., 2015).
(d) Only nighttime measurements are used.

A comparison of the resulting frequency distributions is shown in Fig. 11. Descriptive statistics of the iATB values measured by each lidar are given in Table 2. In both Fig. 11 and Table 2, the mean CATS iATB is seen to underestimate CALIOP by ~11.8%. However, direct comparisons of mean iATB measured in opaque cirrus cannot fully characterize the calibration differences between the two instruments. In particular, any comprehensive evaluation must consider differences in the contributions of multiple scattering to the backscattered signals. Instrument-specific causes for these differences include different laser spot sizes, different receiver fields of view, and different orbit altitudes.

The iATB for opaque layers can be expressed in terms of the layer extinction-to-backscatter ratio, S (more commonly known as the lidar ratio), and a dimensionless, instrument-specific multiple scattering factor, η, using Platt's equation (Platt, 1973):

$$iATB = \frac{1}{2\eta S}. \tag{18}$$

Aggregating 10 months of nighttime measurements acquired within the same time frame and latitude limits yields very large sample sizes for both data sets, so we can reasonably assume that the distribution of lidar ratios observed by CATS and CALIOP are essentially identical. But we cannot assume that the CATS and CALIOP multiple scattering factors are identical, as they depend not only on the phase functions of the measurement targets (in this case, cirrus clouds) but also on instrument design and viewing geometry (Winker, 2003). As mentioned in Sect. 3, the value of η for CATS ($\eta_{\mathrm{CATS}} = 0.52$) has been determined empirically via comparisons to coincident CPL measurements. The cirrus multiple scattering factors applied in the CALIOP V4.10 data release were also determined empirically using extensive coincident measurements made by the CALIPSO infrared imaging radiometer (Garnier et al., 2015). Unlike CATS, η_{CALIOP} is not a fixed constant, but is instead implemented as a function of cloud temperature.

For the opaque cirrus clouds sampled by CALIOP in this study, $\eta_{\mathrm{CALIOP}} = 0.55 \pm 0.06$. Assuming that both instrument teams have accurately characterized cirrus multiple scattering effects on their respective systems, enforcing the assumption that the lidar ratio distributions observed by CATS and CALIOP are essentially identical, we can establish the relative difference in attenuated backscatter measurements between the two lidars using $(iATB_{\mathrm{CALIOP}} \times \eta_{\mathrm{CALIOP}}) / (iATB_{\mathrm{CATS}} \times \eta_{\mathrm{CATS}}) = (0.0313 \times 0.55) / (0.0280 \times 0.52) = 1.182$. This result is consistent with the previous PollyXT comparisons. In "clear air" regions, CATS V3-00

L1B data products underestimates PollyXT measurements of ATB by ~19.7%. In opaque cirrus, CATS V3-00 L1B data products underestimates CALIOP measurements of iATB by ~18.2%

5 Conclusion

This study presents a detailed discussion of the CATS 1064 nm calibration algorithm, as well as validation using three different data sources. Cloud and aerosol layers have strong backscatter intensities and high SNR, so the CATS 1064 nm ATB uncertainties in these layers are primarily related to the uncertainties in the CATS calibration. At night, CATS V3-00 median 1064 nm ATB relative uncertainty is 7% in cloud and aerosol layers, consistent with the estimated 7-10% uncertainty in the Rayleigh normalization technique. The daytime cirrus cloud calibration transfer technique has an estimated uncertainty of 16-18%. CATS V3-00 median daytime 1064 nm ATB relative uncertainty is 21% in cloud and aerosol layers. Coincident flights with the airborne CPL instrument showed that even in conditions with peak solar background noise and lowest SNR, CATS data agrees to within 25% with CPL. The CATS ATB was also compared with the ground based EARLINET systems and found to be overall within 20% of the calibrated EARLINET data. Finally, CATS was compared in a statistical sense with CALIOP, another spaceborne lidar utilizing a different 1064 nm calibration method than CATS, and also found ATB agreement to ~18%. The comparisons between CATS, CPL, Polly^{XT}, and CALIOP 1064 nm ATB fall within the combined estimated uncertainties for the all the instruments. The results shown in this paper give greater confidence in the use of CATS 1064 nm data, especially nighttime data, for a variety of studies investigating cloud and aerosol properties. To date, the CATS data have been used for various applications, including volcanic plume transport (Hughes et al 2016), above cloud aerosol properties (Rajapakshe et al. 2017), cloud diurnal variability (Noel et al. 2018), and diurnal variability of aerosol properties (Lee et al. 2018).

CATS has demonstrated that direct calibration of 1064 nm from spaceborne lidar is possible given the appropriate instrument design and orbit. The CATS design and ISS orbit yielded data that exhibits high nighttime SNR, enabling the direct calibration of the nighttime CATS 1064 nm ATB by normalizing the signal to the Rayleigh profile. The primary strength of this technique is that it does not require assumptions about cirrus 1064-532 nm backscatter color ratios, as is the case with the CALIOP 1064 nm calibration technique (Vaughan et al., 2019). The accuracy of the Rayleigh normalization technique, which is also used for CALIOP 532 nm data, is dependent on an accurate estimate of the aerosol loading in the calibration altitude region. A weakness of the CATS 1064 nm Rayleigh normalization technique is that assumptions about the 1064-532 nm backscatter color ratio for stratospheric aerosols is used because accurate measurements of the 1064 nm aerosol loading in the 22-26 km altitude region, which has higher aerosol loading than the 36-39 km region used for CALIOP, were not available in same timeframe as CATS operations. To improve the calibration of future space-based lidar missions, especially at 1064 nm, a higher calibration altitude region and/or coincident stratospheric aerosol measurements at the same wavelength should be prioritized. Implementing these into a mission design would likely reduce the calibration uncertainties by a factor of two, which would then improve the accuracy of the resulting layer information and aerosol/cloud optical properties derived from the calibrated signal. Accurate backscatter lidar data is critical to improve our understanding of various physical properties of the atmosphere, specifically how clouds and aerosols radiatively impact our earth in the infrared.

Acknowledgements

The CATS instrument was funded by the ISS NASA Research Office (NRO), with CATS data products and processing algorithms funded by NASA Science Mission Directorate (SMD). CATS data products are archived through the Atmospheric Science Data Center (ASDC). CATS browse images and data products are also freely distributed via the CATS web site at http://cats.gsfc.nasa.gov/data/. EARLINET acknowledges support from the European Union's Horizon 2020 research and innovation programme under grant agreements No 654109.

https://doi.org/10.5194/amt-2019-172
Preprint. Discussion started: 12 June 2019

References

Ansmann, A., Riebesell, M., Wandinger, U., Weitkamp, C., Voss, E., Lahmann, W., and Michaelis, W.: Combined Raman elastic backscatter LIDAR for vertical profiling of moisture, aerosol extinction, backscatter, and LIDAR ratio, Appl. Phys., B55, 18–28, doi.org/10.1007/BF00348608, 1992.

Avery, M., Winker, D., Heymsfield, A. J., Vaughan, M., Hu, Y., and Trepte, C.: Cloud ice water content retrieved from the CALIOP space-based lidar, Geophys. Res. Lett., 39, L05808, doi:10.1029/2011GL050545, 2012.

Baars, H., Kanitz, T., Engelmann, R., Althausen, D., Heese, B., Komppula, M., Preißler, J., Tesche, M., Ansmann, A., Wandinger, U., Lim, J.-H., Ahn, J. Y., Stachlewska, I. S., Amiridis, V., Marinou, E., Seifert, P., Hofer, J., Skupin, A., Schneider, F., Bohlmann, S., Foth, A., Bley, S., Pfüller, A., Giannakaki, E., Lihavainen, H., Viisanen, Y., Hooda, R. K., Pereira, S. N., Bortoli, D., Wagner, F., Mattis, I., Janicka, L., Markowicz, K. M., Achtert, P., Artaxo, P., Pauliquevis, T., Souza, R. A. F., Sharma, V. P., van Zyl, P. G., Beukes, J. P., Sun, J., Rohwer, E. G., Deng, R., Mamouri, R.-E., and Zamorano, F.: An overview of the first decade of Polly^{NET}: an emerging network of automated Raman-polarization lidars for continuous aerosol profiling, Atmos. Chem. Phys., 16, 5111-5137, doi.org/10.5194/acp-16-5111-2016, 2016.

Campbell, J. R., Vaughan, M. A., Oo, M., Holz, R. E., Lewis, J. R., and Welton, E. J.: Distinguishing cirrus cloud presence in autonomous lidar measurements, Atmos. Meas. Tech., 8, 435–449, doi.org/10.5194/amt-8-435-2015, 2015.

Collins R. T. H., Russell P. B.: Lidar measurement of particles and gases by elastic backscattering and differential absorption, Laser Monitoring of the Atmosphere, in: Topics in Applied Physics, 14, edited by: Hinkley, E. D., Springer-Verlag, Berlin, 71-151, doi:10.1007/3-540-07743-X_18, 1976.

D'Amico, G., Amodeo, A., Baars, H., Binietoglou, I., Freudenthaler, V., Mattis, I., Wandinger, U., and Pappalardo, G.: EARLINET Single Calculus Chain – overview on methodology and strategy, Atmos. Meas. Tech., 8, 4891–4916, doi:10.5194/amt-8- 4891-2015, 2015.

D'Amico, G., Amodeo, A., Mattis, I., Freudenthaler, V., and Pap-palardo, G.: EARLINET Single Calculus Chain – technical – Part1: Pre-processing of raw lidar data, Atmos. Meas. Tech., 9, 491–507, doi:10.5194/amt-9-491-2016, 2016.

Del Guasta, M.: Errors in the retrieval of thin cloud optical parameters obtained with a two boundary algorithm, Appl. Opt., 37, 5522–5540, 1998.

Engelmann, R., Kanitz, T., Baars, H., Heese, B., Althausen, D., Skupin, A., Wandinger, U., Komppula, M., Stachlewska, I. S., Amiridis, V., Marinou, E., Mattis, I., Linné, H., and Ansmann, A.: The automated multiwavelength Raman polarization and water-vapor lidar Polly^{XT}: the neXT generation, Atmos. Meas. Tech., 9, 1767-1784, https://doi.org/10.5194/amt-9-1767-2016, 2016.

Fernald, F.: Analysis of atmospheric lidar observations- Some comments, Appl. Optics, 23(5), 652-653, doi:10.1364/AO.23.000652, 1984.

Garnier, A., Pelon, J., Vaughan, M. A., Winker, D. M., Trepte, C. R., and Dubuisson, P.: Lidar multiple scattering factors inferred from CALIPSO lidar and IIR retrievals of semi-transparent cirrus cloud optical depths over oceans, Atmos. Meas. Tech., 8, 2759–2774, https://doi.org/10.5194/amt-8-2759-2015, 2015.

Gelaro, R., McCarty, W., Suárez, M. J., Todling, R., Molod, A., Takacs, L., Randles, C. A., Darmenov, A., Bosilovich, M. G., Reichle, R., Wargan, K., Coy L., Cullather, R., Draper, C., Akella, S., Buchard, V., Conaty, A., da Silva, A. M., Gu, W., Kim, G., Koster, R., Lucchesi, R., Merkova, D., Nielsen, J. E., Partyka, G., Pawson, S., Putman, W., Rienecker, M., Schubert, S. D., Sienkiewicz, M., and Zhao, B.: The Modern-Era Retrospective Analysis for Research and Applications, Version 2 (MERRA-2). *J. Climate,* 30, 5419–5454, https://doi.org/10.1175/JCLI-D-16-0758.1, 2017.

Haarig, M., Ansmann, A., Althausen, D., Klepel, A., Groß, S., Freudenthaler, V., Toledano, C., Mamouri, R.-E., Farrell, D. A., Prescod, D. A., Marinou, E., Burton, S. P., Gasteiger, J., Engelmann, R., and Baars, H.: Triple-wavelength depolarization-ratio profiling of Saharan dust over Barbados during SALTRACE in 2013 and 2014, Atmos. Chem. Phys., 17, 10767-10794, https://doi.org/10.5194/acp-17-10767-2017, 2017.

Haarig, M., Engelmann, R., Ansmann, A., Veselovskii, I., Whiteman, D. N., and Althausen, D.: 1064 nm rotational Raman lidar for particle extinction and lidar-ratio profiling: cirrus case study, Atmos. Meas. Tech., 9, 4269-4278, https://doi.org/10.5194/amt-9-4269-2016, 2016.

Hair, J. W., Hostetler, C. A., Cook, A. L., Harper, D. B., Ferrare, R. A., Mack, T. L., Welch, W., Izquierdo, L. R., and Hovis, F. E.: Airborne High Spectral Resolution Lidar for profiling aerosol optical properties, Appl. Optics, 47, 6734–6752, doi:10.1364/AO.47.006734, 2008.

Holben, B. N., Eck, T. F., Slutsker, I., Tanre, D., Buis, J. P., Setzer, A., Vermote, E., Reagan, J. A., Kaufman, Y., Nakajima, T., Lavenue, F., Jankowiak, I., and Smirnov, A.: AERONET – A federated instrument network and data archive for aerosol characterization, Remote Sens. Environ., 66, 1–16, https://doi.org/10.1016/S0034-4257(98)00031-5, 1998.

Hostetler, C. A., Liu, Z., Reagan, J. A., Vaughan, M. A., Winker, D. M., Osborn, M. T., Hunt, W. H., Powell, K. A., and Trepte, C. R.: CALIPSO algorithm theoretical basis document, PC-SCI-201. https://www-calipso.larc.nasa.gov/resources/project_documentation.php, 2005.

Hughes, E. J., Yorks, J. E., Krotkov, N. A., da Silva. A. M., and McGill, M.: Using CATS near-realtime lidar observations to monitor and constrain volcanic sulfur dioxide (SO_2) forecasts, Geophys. Res. Lett., 43, *doi:*10.1002/2016GL070119. 2016, 2016.

Hunt, W. H., Winker, D. M., Vaughan, M. A., Powell, K. A., Lucker, P. L., and Weimer, C.: CALIPSO lidar description and performance assessment, J. Atmos. Oceanic Technol., 26, 1214–1228, doi:10.1175/ 2009JTECHA1223.1, 2009.

Iqbal, M.: An Introduction to Solar Radiation, Academic Press, New York, NY, 1983.

Kar, J., Vaughan, M. A., Lee, K.-P., Tackett, J. L., Avery, M. A., Garnier, A., Getzewich, B. J., Hunt, W. H., Josset, D., Liu, Z., Lucker, P. L., Magill, B., Omar, A. H., Pelon, J., Rogers, R. R., Toth, T. D., Trepte, C. R., Vernier, J.-P., Winker, D. M., and Young, S. A.: CALIPSO lidar calibration at 532 nm: version 4 nighttime algorithm, Atmos. Meas. Tech., 11, 1459-1479, https://doi.org/10.5194/amt-11-1459-2018, 2018.

Klett, J.: Stable analytical inversion solution for processing lidar returns, Appl. Optics, 20(2), 211-220, doi:10.1364/AO.20.000211, 1981.

Lee, L., Zhang, J., Reid, J. S., and Yorks, J. E.: Investigation of CATS aerosol products and application toward global diurnal variation of aerosols, Atmos. Chem. Phys. Discuss., https://doi.org/10.5194/acp-2018-1298, in review, 2018.

Liou, K. N., Takano, Y., and Yang, P.: Light scattering and radiative transfer in ice crystal clouds: Applications to climate research, in Light Scattering by Nonspherical Particles, edited by M. Mishchenko, J. W. Hovenier, and L. D. Travis, pp. 417–449, Academic, San Diego, Calif., 2000.

Liu, Z., McGill, M., Hu, Y., Hostetler, C. A., Vaughan, M., and Winker, D.: Validating lidar depolarization calibration using solar radiation scattered by ice clouds, IEEE Geosci. Remote Sens. Lett.,1, doi:10.1109/LGRS.2004.829613, 2004.

Mamouri, R. E., Amiridis, V., Papayannis, A., Giannakaki, E., Tsaknakis, G., and Balis, D. S.: Validation of CALIPSO space-borne-derived attenuated backscatter coefficient profiles using a ground-based lidar in Athens, Greece, Atmos. Meas. Tech., 2, 513-522, https://doi.org/10.5194/amt-2-513-2009, 2009.

Mattis, I., D'Amico, G., Baars, H., Amodeo, A., Madonna, F., and Iarlori, M.: EARLINET Single Calculus Chain – technical – Part 2: Calculation of optical products, Atmos. Meas. Tech., 9, 3009-3029, https://doi.org/10.5194/amt-9-3009-2016, 2016.

McGill, M.J., Hlavka, D. L., Hart, W. D., Spinhirne, J. D., Scott, V. S., and Schmid, B.: The Cloud Physics Lidar: Instrument description and initial measurement results, Appl. Optics, 41, https://doi.org/10.1364/AO.41.003725, 2002.

McGill, M. J., Hlavka, D. L., Hart, W. D., Welton, E. J., and Campbell, J. R.: Airborne lidar measurements of aerosol optical properties during SAFARI-2000, J. Geophys. Res., 108, 8493, doi: 10.1029/2002JD002370, D13, 2003.

McGill, M.J., Vaughan, M. A., Trepte, C. R., Hart, W. D., Hlavka, D. L., Winker, D. M, and Keuhn, R.: Airborne validation of spatial properties measured by the CALIPSO lidar, J. Geophys. Res., 112, doi: 10.1029/2007JD008768, 2007.

McGill, M. J., Yorks, J. E., Scott, V. S., Kupchock, A. W., and Selmer, P. A.: The Cloud-Aerosol Transport System (CATS): A technology demonstration on the International Space Station, Proceedings of the SPIE 9612, Lidar Remote Sensing for Environmental Monitoring XV, 96120A, 17 September 2015, https://doi.org/10.1117/12.2190841, 2015.

Mona, L., Pappalardo, G., Amodeo, A., D'Amico, G., Madonna, F., Boselli, A., Giunta, A., Russo, F., and Cuomo, V.: One year of CNR-IMAA multi-wavelength Raman lidar measurements in correspondence of CALIPSO overpass: Level 1 products comparison, Atmos. Chem. Phys., 9, doi:10.5194/acpd-9-8429-2009, 2009.

Noel, V., Chepfer, H., Chiriaco, M., and Yorks, J.: The diurnal cycle of cloud profiles over land and ocean between 51° S and 51° N, seen by the CATS spaceborne lidar from the International Space Station, Atmos. Chem. Phys. Discuss., https://doi.org/10.5194/acp-2018-214, 2018.

Papagiannopoulos, N., Mona, L., Alados-Arboledas, L., Amiridis, V., Baars, H., Binietoglou, I., Bortoli, D., D'Amico, G., Giunta, A., Guerrero-Rascado, J. L., Schwarz, A., Pereira, S., Spinelli, N., Wandinger, U., Wang, X., and Pappalardo, G.: CALIPSO climatological products: evaluation and suggestions from EARLINET, Atmos. Chem. Phys., 16, 2341-2357, https://doi.org/10.5194/acp-16-2341-2016, 2016.

Papayannis, A., Mamouri, R. E., Amiridis, V., Kazadzis, S., Pérez García-Pando, C., Tsaknakis, G., Kokkalis, P., Baldasano, J.: Systematic lidar observations of Saharan dust layers over Athens, Greece in the frame of EARLINET project (2004-2006). Annales Geophysicae. 27, 3611-3620, doi:10.5194/angeo-27-3611, 2009.

Platt, C. M.: Lidar and radiometric observations of cirrus clouds. J. Atmos. Sci., 30, 1191–1204, https://doi.org/10.1175/1520-0469, 1973.

Platt, C. M.: Remote sounding of high clouds: I. Calculation of visible and infrared optical properties from lidar and radiometer measurements, J. App. Met., 18, 1130-1143, doi.org/10.1175/1520-0450, 1979.

Povey, A. C., Grainger, R. G., Peters, D. M., and Agnew, J. L.: Retrieval of aerosol backscatter, extinction, and lidar ratio from Raman lidar with optimal estimation, Atmos. Meas. Tech., 7, 757-776, https://doi.org/10.5194/amt-7-757-2014, 2014.

Powell, K. A., Hostetler, C. A., Liu, Z., Vaughan, M. A., Kuehn, R. E., Hunt, W. H., Lee, K., Trepte, C. R., Rogers, R. R., Young, S. A., and Winker, D. M.: CALIPSO Lidar Calibration Algorithms: Part I - Nighttime 532 nm Parallel Channel and 532 nm Perpendicular Channel, J. Atmos. Oceanic Technol., 26, 2015–2033, 2009.

Proestakis, E., Amiridis, V., Marinou, E., Binietoglou, I., Ansmann, A., Wandinger, U., Hofer, J., Yorks, J., Nowottnick, E., Makhmudov, A., Papayannis, A., Pietruczuk, A., Gialitaki, A., Apituley, A., Szkop, A., Muñoz Porcar, C., Bortoli, D., Dionisi, D., Althausen, D., Mamali, D., Balis, D., Nicolae, D., Tetoni, E., Liberti, G. L., Baars, H., Mattis, I., Stachlewska, I., Voudouri, K. A., Mona, L., Mylonaki, M., Perrone, M. R., Costa, M. J., Sicard, M., Papagiannopoulos, N., Siomos, N., Burlizzi, P., Pauly, R., Engelmann, R., Abdullaev, S., and Pappalardo, G.: EARLINET evaluation of the CATS L2 aerosol backscatter coefficient product, Atmos. Chem. Phys. Discuss., https://doi.org/10.5194/acp-2019-45, in review, 2019.

Rajapakshe, C., Zhang, Z., Yorks, J. E., Yu, H., Tan, Q., Meyer, K., and Platnick., S.: Seasonally transported aerosol layers over southeast Atlantic are closer to underlying clouds than previously reported, Geophys. Res. Lett., 44, doi:10.1002/2017GL073559, 2017.

Reagan, J. A., Wang, X., and Osborn, M. T.: Spaceborne lidar calibration from cirrus and molecular backscatter returns, in: IEEE Transactions on Geoscience and Remote Sensing, vol. 40, no. 10, pp. 2285-2290, doi: 10.1109/TGRS.2002.802464, 2002.

Russell, P. B., Swissler, T. J., and McCormick, M. P.: Methodology for error analysis and simulation of lidar aerosol measurements, Appl. Opt. 18, 3783-3797, 1979.

Spinhirne, J. D., Palm, S. P., Hart, W. D., Hlavka, D. L., and Welton, E. J.: Cloud and aerosol measurements from GLAS: Overview and initial results, Geophys. Res. Lett., 32, L22S03, doi:10.1029/2005GL023507, 2005.

Vaughan, M. A., Liu, Z., McGill, M. J., Hu, Y., and Obland, M. D.: On the Spectral Dependence of Backscatter from Cirrus Clouds: Assessing CALIOP's 1064 nm Calibration Assumptions Using Cloud Physics Lidar Measurements, J. Geophys. Res., 115, D14206, https://doi.org/10.1029/2009JD013086, 2010.

Vaughan, M., Garnier, A., Josset, D., Avery, M., Lee, K.-P., Liu, Z., Hunt, W., Pelon, J., Hu, Y., Burton, S., Hair, J., Tackett, J. L., Getzewich, B., Kar, J., and Rodier, S.: CALIPSO lidar calibration at 1064 nm: version 4 algorithm, Atmos. Meas. Tech., 12, 51–82, https://doi.org/10.5194/amt-12-51-2019, 2019.

Vernier, J. P., Pommereau, J. P., Garnier, A., Pelon, J., Larsen, N., Nielsen, J., Christiansen, T., Cairo, F., Thomason, L. W., Leblanc, T., and McDermid, I. S.: Tropical stratospheric aerosol layer from CALIPSO lidar observations, J. Geophys. Res., 114, D00H10, https://doi.org/10.1029/2009JD011946, 2009.

Welton, E. J., Campbell, J. R., Spinhirne, J. D., Scott, V. S.: Global monitoring of clouds and aerosols using a network of micropulse lidar systems, in: Proc. SPIE 4153, Lidar Remote Sensing for Industry and Environment Monitoring, 13 February 2001, doi:10.1117/12.417040, 2001.

Welton, E. J. and Campbell, J. R.: Micropulse Lidar Signals: Uncertainty analysis. *J. Atmos. Oceanic Technol.,* **19**, 2089–2094, https://doi.org/10.1175/1520-0426(2002)019<2089:MLSUA>2.0.CO;2, 2002.

Welton, E. J., Voss, K. J., Quinn, P. K., Flatau, P. J., Markowicz, K., Campbell, J. R., Spinhirne, J. D., Gordon, H. R., and Johnson, J. E.: Measurements of aerosol vertical profiles and optical properties during INDOEX 1999 using micropulse lidars, J. Geophys. Res.,107,8019, doi:10.1029/2000JD000038, 2002.

Whiteman, D. N.: Examination of the traditional Raman lidar technique. 1. Evaluating the temperature-dependent lidar equations, Appl. Optics, 42(15), 2571–2592, doi:10.1364/AO.42.002571, 2003.

Winker, D.: Accounting for multiple scattering in retrievals from space lidar, Proc. SPIE, 5059, 128–139, 2003.

Winker, D. M, Couch, R. H., and McCormick, P. M.: An overview of LITE: NASA's Lidar In-space Technology Experiment. Proc. IEEE.,84**,** 1–17, 1996.

Winker, D.M., Pelon, J., Coakley, J. A., Ackerman, S. A., Charlson, R. J., Colarco, P. R., Flamant, P., Fu, Q., Hoff, R. M., Kittaka, C., Kubar, T. L., Le Treut, H., Mccormick, P. M., Mégie, G., Poole, L., Powell, K., Trepte, C., Vaughan, M. A., and Wielicki, B. A.,: The CALIPSO Mission. Bull. Amer. Meteor. Soc., 91, 1211–1230, https://doi.org/10.1175/2010BAMS3009.1, 2010.

Yorks, J. E., Hlavka, D. L., Hart, W. D., and McGill, M. J.: Statistics of Cloud Optical Properties from Airborne Lidar Measurements. J. Atmos. Oceanic Technol., 28, 869–883, https://doi.org/10.1175/2011JTECHA1507.1, 2011.

Yorks, J. E., McGill, M. J., Palm, S. P., Hlavka, D. L., Selmer, P. A., Nowottnick, E. P., Vaughan, M. A., Rodier, S. D., and Hart, W. D.: An overview of the CATS level 1 processing algorithms and data products, Geophys. Res. Lett., 43, 4632–4639, doi:10.1002/2016GL068006, 2016a.

Yorks, J. E., Palm, S. P., Hlavka, D. L., McGill, M. J., Nowottnick, E., Selmer, P., and Hart, W. D.: The Cloud-Aerosol Transport System (CATS) algorithm theoretical basis document, http://cats.gsfc.nasa.gov/media/docs/CATS_ATBD.pdf, 2016b.

Yorks, J. E., Nowottnick, E., Selmer, P. A., Rodier, S. D., Vaughan, M. A, Dacic, N., McGill, M. J., and Palm, S. P..: CATS level 2 vertical feature mask algorithms and data products: An overview and initial assessment, Atmos. Meas. Tech. Discuss., in preparation.

Young, S. A., Vaughan, M. A., Garnier, A., Tackett, J. L., Lambeth, J. D., and Powell, K. A.: Extinction and optical depth retrievals for CALIPSO's Version 4 data release, Atmos. Meas. Tech., 11, 5701-5727, https://doi.org/10.5194/amt-11-5701-2018, 2018.

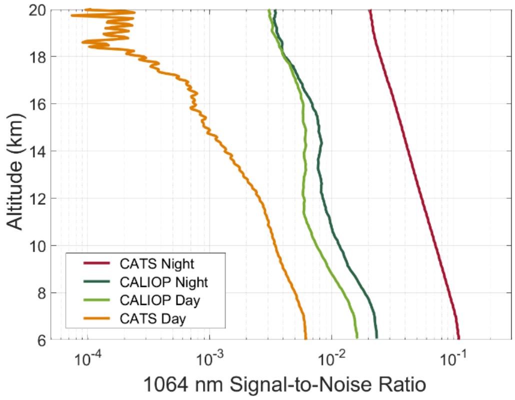

Figure 1: The CATS and CALIOP 1064 nm signal to noise ratios for both daytime and nighttime data. The CATS nighttime SNR is nearly an order of magnitude greater than CALIOP (day and night), while the CATS daytime SNR is lower than CALIOP. The CATS profiles are computed for data acquired at a laser pulse rate of 4 kHz and averaged to 350 m horizontally. The CALIOP profiles are calculated for individual laser pulses acquired at 20.16 Hz, equivalent to a horizontal resolution of 335 m. The initial vertical resolution for all profiles is 60 m. All profiles are subsequently smoothed using a 2-km (34 point) running average.

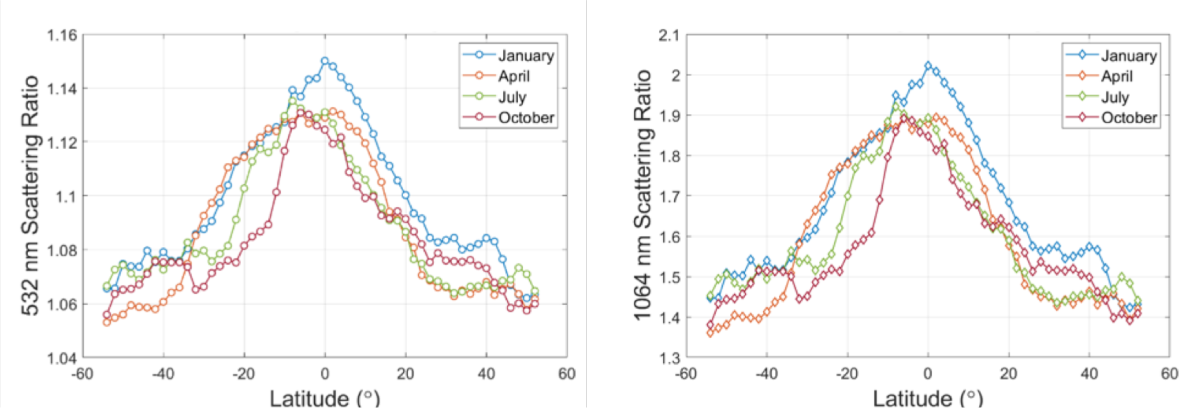

Figure 2: The 532 nm scattering ratios measured by CALIOP within the CATS calibration region (left) and the 1064 nm scattering ratios estimated from the 532 nm retrievals (right) from 2016. These plots show the temporal and latitudinal variability within the calibration region where 1064 nm estimated scattering ratios can range from below 1.4 to above 2.0 depending on the time of year and geographical location.

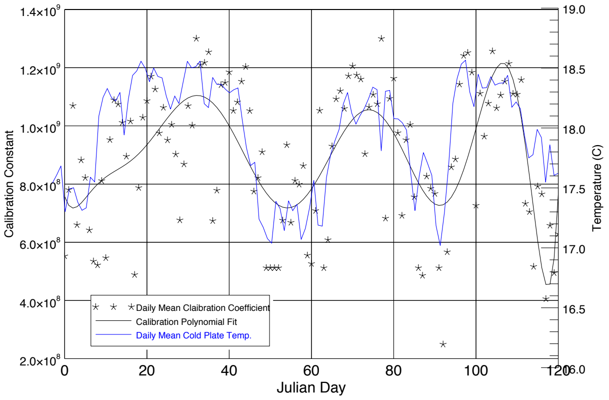

Figure 3: The average CATS nighttime calibration coefficient for each day, polynomial fit of the average calibration coefficient with time, and the daily average cold plate temperature demonstrates the correlation between calibration values and the instrument cold plate temperature. The correlation coefficient between the daily average calibration coefficient and cold plate temperature is 0.8066.

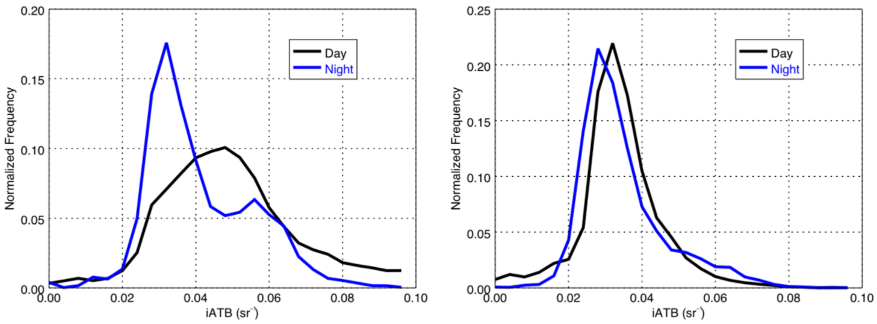

Figure 4: Distributions of CATS thin (physical thickness < 2 km), opaque cirrus iATB distributions from V2-01 (left) and V3-00 (right). These plots demonstrate the CATS daytime calibration method using calibration transfer from the nighttime calibration.

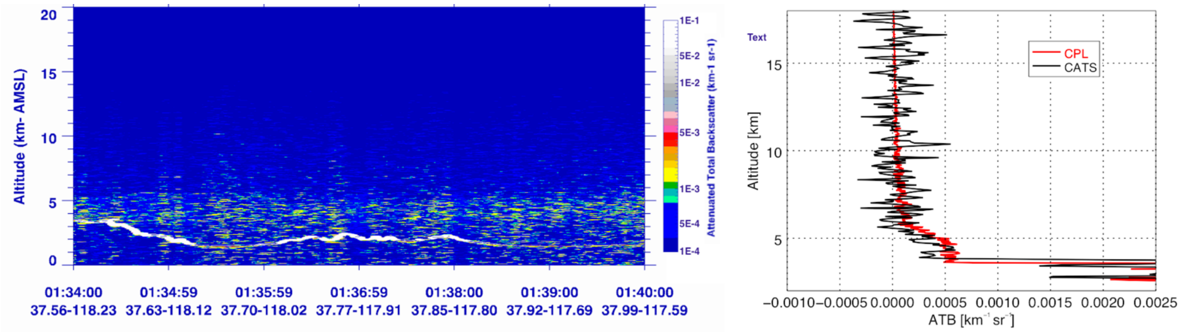

Figure 5: The CPL curtain plot of ATB centered around the 01:37 UTC coincident point from the 7-8 August 2015 CCAVE flight (Left). The mean ATB profiles from CATS and CPL during this under flight (right).

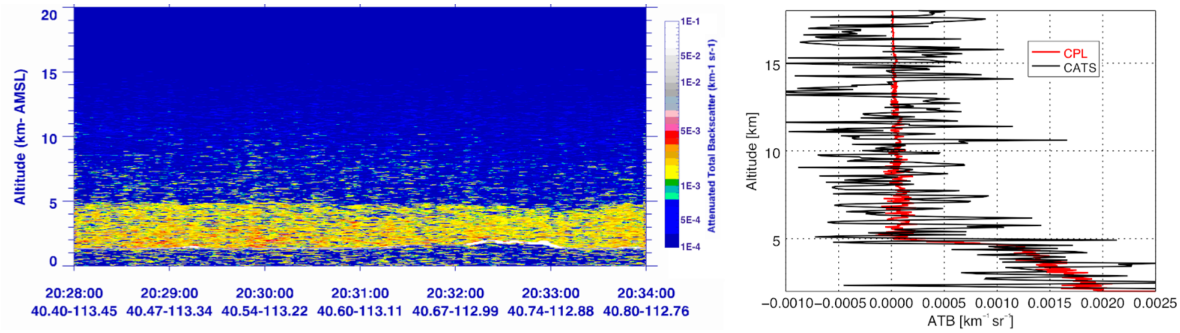

Figure 6: The 20 August 2015 CATS/CPL coincident flight. The CPL 70 km coincident segment curtain plot (left) was used to compute the mean ATB profile (right) from CPL along the same path as CATS. The CATS and CPL data show good agreement despite higher noise levels in the CATS profile due to daytime retrieval limitations.

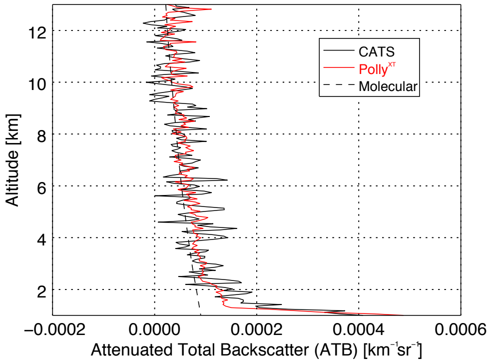

Figure 7: The mean CATS and Polly^{XT} ATB profiles from the CATS overpass of the Leipzig, Germany EARLINET site at 01:13:34 UTC on 24 September 2015. CATS passed within 31 km of the EARLINET site.

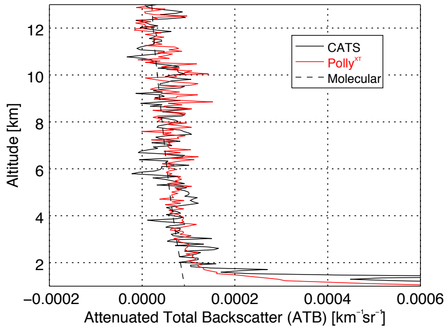

Figure 8: The mean CATS and Polly^{XT} ATB profiles from the CATS overpass of the Leipzig, Germany EARLINET site at 00:18:19 UTC on 30 July 2015. CATS passed within 41 km of the EARLINET site.

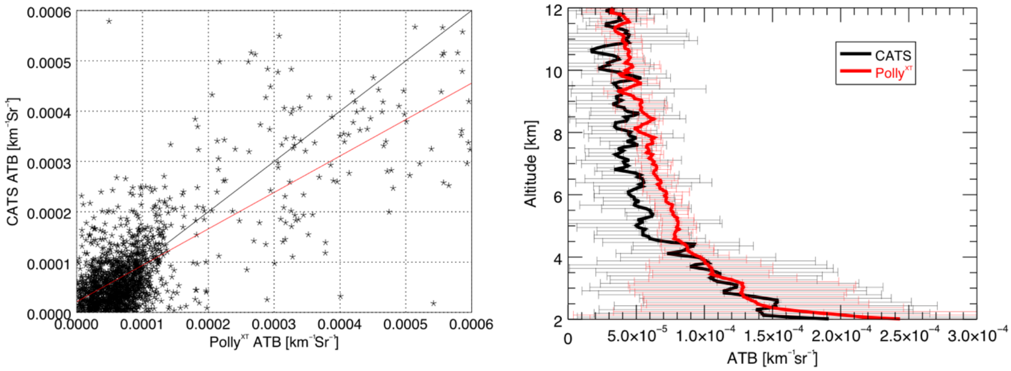

Figure 9: Scatter plot of all eight Polly^{XT} /CATS comparison overflights (left). The black line is the one-to-one line while the red line is the line fit of the data set. The correlation coefficient is 0.75. The average ATB profile from all eight Polly^{XT}/CATS comparison cases (right) shows the CATS mean profile is on average 19.67% lower than Polly^{XT} from 3-12 km. The horizontal lines show the standard deviations of the mean profile for both CATS and Polly^{XT}.

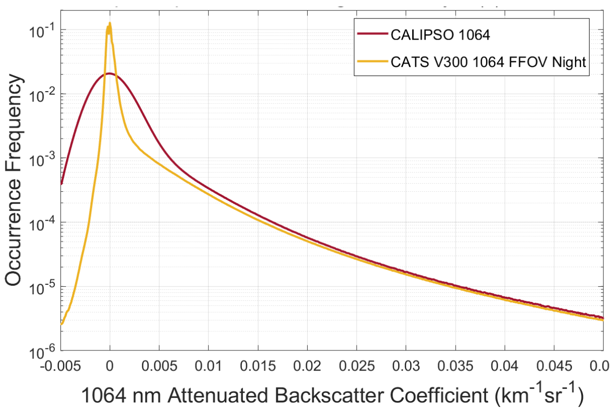

Figure 10: Frequency distributions of 1064 nm attenuated backscatter coefficients measured by CALIOP (V4.10) and CATS (V3-00) from April through September 2016 at night with temperatures less than -40 C.

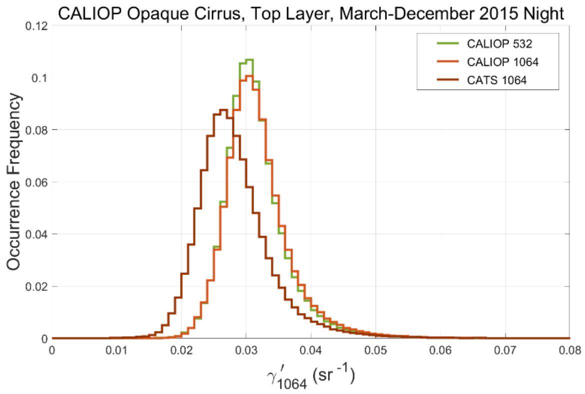

Figure 11: Frequency distributions of March-December 2015 nighttime integrated attenuated backscatter for opaque cirrus clouds measured by CALIOP at 532 nm and 1064 nm and by CATS at 1064 nm only.

	Night	Day	Mean Bias (Night-Day)	MAE
Mean	0.03840	0.03823	0.000168	0.003419
Median	0.03559	0.03681	-0.001215	0.003289
Standard Dev.	0.01386	0.01390	$-3.969e^{-5}$	0.002430
Mode	0.02981	0.03239	-0.00258	0.00413

Table 1: Mean, median, mode and standard deviation of the day and night iATB distributions of geometrically thin, opaque cirrus clouds from all V3-00 CATS data. The mean bias, and mean absolute error (MAE) were also calculated between the day and night distributions.

	CALIOP 532 nm	CALIOP 1064 nm	CATS 1064 nm
minimum	0.0017 sr^{-1}	0.0015 sr^{-1}	0.0001 sr^{-1}
maximum	0.1189 sr^{-1}	0.1248 sr^{-1}	0.1794 sr^{-1}
median	0.0303 sr^{-1}	0.0305 sr^{-1}	0.0270 sr^{-1}
MAD	0.0036 sr^{-1}	0.0038 sr^{-1}	0.0045 sr^{-1}
mean	0.0310 sr^{-1}	0.0313 sr^{-1}	0.0280 sr^{-1}
standard deviation	0.0050 sr^{-1}	0.0053 sr^{-1}	0.0071 sr^{-1}
samples	333,228	333,228	268,806

Table 2: descriptive statistics for the integrated attenuated backscatter of opaque cirrus clouds detected during nighttime granules by CATS and CALIOP during the period from 1 March to 31 December 2015 (MAD = median absolute distance).